A Review on Recent Advances in Doppler Radar Sensors for Noncontact Healthcare Monitoring

Changzhi Li, *Member, IEEE,* Victor M. Lubecke, *Senior Member, IEEE,*
Olga Boric-Lubecke, *Senior Member, IEEE,* and Jenshan Lin, *Fellow, IEEE*

(Invited Paper)

Abstract—This paper reviews recent advances in biomedical and healthcare applications of Doppler radar that remotely detects heartbeat and respiration of a human subject. In the last decade, new front-end architectures, baseband signal processing methods, and system-level integrations have been proposed by many researchers in this field to improve the detection accuracy and robustness. The advantages of noncontact detection have drawn interests in various applications, such as energy smart home, baby monitor, cardiopulmonary activity assessment, and tumor tracking. While many of the reported systems were bench-top prototypes for concept verification, several portable systems and integrated radar chips have been demonstrated. This paper reviews different architectures, baseband signal processing, and system implementations. Validations of this technology in a clinical environment will also be discussed.

Index Terms—Cardiopulmonary, Doppler radar, healthcare, heartbeat, noncontact measurement, respiration, sensor, vital sign.

I. INTRODUCTION

DOPPLER radar has been widely used in a number of applications, including vehicle speed measurement and storm tracking. The same principle, detecting the frequency or phase shift in a reflected radar signal, can be used to detect tiny physiological movements induced by breathing and heartbeat, without any sensor attached to the body. This noncontact remote detection of vital signs lead to several potential applications, such as searching for survivors after earthquake and monitoring sleeping infants or adults to detect abnormal breathing condition. While the concept of noncontact detection of vital signs has been successfully demonstrated by pioneers in this field before 2000 [1]–[5], research efforts in this century have been moving the technology development toward lower power, lighter weight, smaller form factor, better accuracy,

longer detection range, and more robust operation for practical portable and handheld applications. Among the many possible applications this technology can be used for, healthcare seems to be drawing most of the interests [6]. As an example, a baby monitor using this technology was recently demonstrated to monitor Sudden Infant Death Syndrome (SIDS), which is the third leading cause of infant mortality [7]–[9]. The Doppler radar embedded into the baby monitor detects tiny baby movements induced by breathing. If no movement is detected within 20 s, an alarm goes off to warn the parents. Operating in similar ways, biomedical Doppler radar is also being investigated as a cost-effective solution for long-term monitoring of sleep apnea without intervening with the normal life styles of patients [10]. Human studies in clinical environment have validated this technology as a potential substitute for conventional respiratory monitors [11], [12] and a useful tool for precise assessment of key parameters relating to cardiopulmonary activity [13]. Furthermore, recent studies have demonstrated that the Doppler radar could assist medical linear accelerator in tracking the location of a mobile tumor during radiotherapy [14], [15]. Doppler radar has also been applied to monitor the health and behavior of land and sea animals including lizards and fish [16]–[18].

With growing interests in health and life sciences in the engineering community, many researchers have been contributing to the technology advancement in this field. This has led to various radar front-end architectures from the conventional homodyne/heterodyne to self-/mutual- injection locking. Each of these architectures shows its specific advantage in certain environments. In the meantime, signal processing methods such as arctangent (AT) demodulation [19], adaptive dc calibration [20], [21], and noise cancellation [22]–[25] have been proposed to tackle potential hindrances for wide practical applications of the biomedical radar. Signal processing techniques, including blind source separation (BSS) and passive RF tags, have been applied as well, to isolate multiple subjects and clutter noise [26], [27]. Various implementations from bench-top fast prototyping using fundamental RF/microwave instruments [28] to radar-on-chip application-specific integrated circuit (ASIC) [29]–[32] have been demonstrated to make this technology available to both researchers and general users. This paper reviews the achievements reported in recent years, especially the last decade, and discusses potential future research areas that will lead to practical adoption of this technology in the daily life of ordinary people.
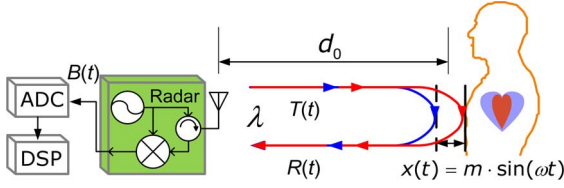
Fig. 1. Fundamental mechanism of CW Doppler radar vital sign detection.

The paper starts with the fundamental theory of continuous wave (CW) Doppler radar for biomedical application in Section II. It then discusses the various architectures of RF front-end in Section III and different baseband demodulation and signal processing methods in Section IV. Some advanced system-level implementation and detection techniques will be reviewed in Section V. The challenges for wide application of this technology in daily life and the potential future research directions will be discussed in Section VI. A conclusion will be drawn in Section VII.

II. CW Doppler Radar for Healthcare Monitoring

A. Detection Theory

Fig. 1 shows the fundamental mechanism of CW Doppler radar vital sign detection. An un-modulated signal $T(t) = \cos[2\pi ft + \Phi(t)]$ with carrier frequency f and phase noise $\Phi(t)$ is transmitted toward a human body at a nominal distance of d_0, where it is phase modulated by the physiological movement $x(t)$ (i.e., heartbeat and respiration). Neglecting amplitude variation, the reflected signal captured by the radar receiver is represented as

$$R(t) \approx \cos\left[2\pi ft - \frac{4\pi d_0}{\lambda} - \frac{4\pi x(t)}{\lambda} + \Phi\left(t - \frac{2d_0}{c}\right)\right] \tag{1}$$

where c is the speed of electromagnetic wave and λ is the wavelength. The received signal is similar to the transmitted signal with a time delay determined by the nominal distance of the target and with its phase modulated by the periodic motion of the target. Using the same transmitted signal $T(t)$ as the local oscillator (LO) signal, the radar receiver down-converts the received signal $R(t)$ into baseband

$$B(t) = \cos\left[\theta + \frac{4\pi x(t)}{\lambda} + \Delta\Phi(t)\right] \tag{2}$$

where $\theta = 4\pi d_0/\lambda + \theta_0$ is determined by the nominal detection distance d_0 and the phase shift θ_0 at the reflection surface. $\Delta\Phi(t) = \Phi(t) - \Phi(t - 2d_0/c)$ is the residual oscillator phase noise.

After analog-to-digital conversion (ADC), the information related to physiological movement can be identified by processing the digitized $B(t)$. Fig. 2 shows an example of the baseband signal and spectrum detected using a CW Doppler radar integrated on a single CMOS chip. The radar chip has a homodyne quadrature architecture, and thus has two output channels (I/Q), as will be discussed in Section III-A.
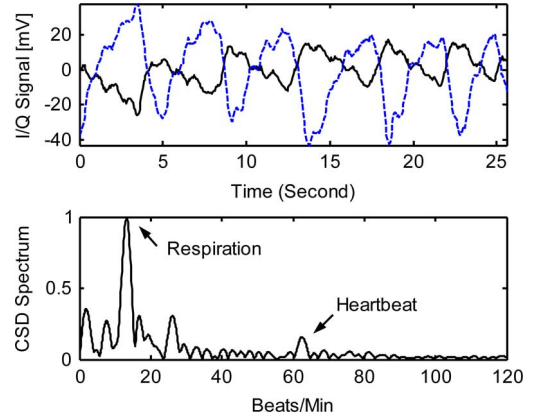

Fig. 2. Baseband: (a) I/Q channel signal and (b) spectrum detected from the front of a human subject at 1.5 m away. From [31].

Since the same transmitted signal is used as the LO to down-convert the received signal, there is no frequency offset in the baseband. The timing delay does not affect the detection either since it only introduces a constant phase shift to the carrier. Therefore, no synchronization mechanism is required for the system. It should be noted that the radar block diagram in Fig. 1 is simplified. For the implementation of robust CW Doppler vital sign detection radar, building blocks such as a low-noise amplifier (LNA), down-conversion mixer, baseband amplifier, and filter are needed. Different front-end architectures can be used for the radar, as will be discussed in later sections.

In radar applications, the phase noise of the LO can mix with the received echo signal and disrupt the desired baseband signal if the phase noise of the two signals entering the mixer is not correlated. Mathematically, it means the $\Delta\Phi(t)$ term in the baseband signal $B(t)$ may disrupt accurate detection of $x(t)$ due to phase noise. This challenge is significantly alleviated by the range-correlation effect at a short detection distance [30]. By using the same transmitted signal as the LO of the down-converter, the LO phase noise is effectively cancelled out, making high sensitivity vital sign detection radar possible.

The choice of carrier frequency is very important. Reference [33] has demonstrated that there exists an optimal carrier frequency for people with different physiological movement strengths. Carrier frequencies ranging from hundreds of megahertz [5] to millimeter-wave frequency [34]–[37] has been tested for noncontact vital sign detection. In [34], a 228-GHz carrier was used for noncontact vital sign detection for three reasons. First, shorter wavelengths provide a greater sensitivity to small displacement. Second, this frequency is in an atmospheric window with at least 50% single-pass transmission [38]. Finally, higher frequency can maintain a collimated beam over much greater distances for reasonable aperture sizes, and the radar cross section of the vital sign area may also increase as frequency increases. This 228-GHz system has successfully extended the respiration and heart rate measurement to a range of 50 m. However, using very high carrier frequency makes it difficult to measure respiration and heartbeat together. The results in [34] only showed the detection of heartbeat while the subject was holding the breath. Nevertheless, the encouraging
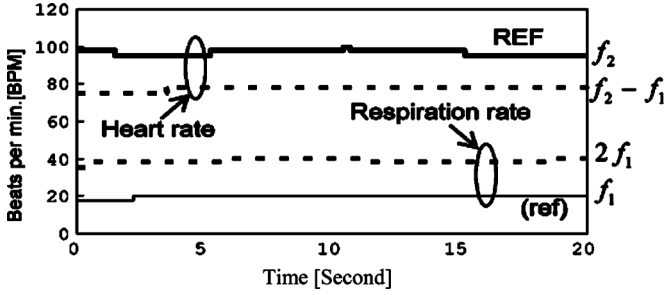
Fig. 3. Measurements of heart and respiration rates taken at a null point. Each measured value is subject to interaction with the other, and so they differ from actual reference values. From [19].

result verified that long-range detection is feasible by using higher carrier frequency.

B. Small Angle Approximation versus Nonlinear Analysis

When the movement amplitude is much smaller than the wavelength λ, a linear approximation can be applied [30]. If θ is an odd multiple of $\pi/2$, the baseband output is approximately

$$B(t) \approx \frac{4\pi x(t)}{\lambda} + \Delta\Phi. \tag{3}$$

In this case, the baseband output is proportional to the motion displacement $x(t)$ and the optimum phase-demodulation sensitivity is achieved. If θ is an even multiple of $\pi/2$, the baseband output is approximately

$$B(t) \approx 1 - \left[\frac{4\pi x(t)}{\lambda} + \Delta\Phi\right]^2. \tag{4}$$

In this case, the baseband output is no longer linearly proportional to the time-varying displacement $x(t)$, and the detection happens at a null-detection point. This null point occurs when the LO and received signal $R(t)$ are either in-phase or 180° out-of-phase. Since the variable part of θ is dependent only on the distance to the target d_0, the null detection point occurs with a target distance every $\lambda/4$ from the radar. Unmanaged null points can result not only in a poor signal, but can actually yield incorrect measurement values. Fig. 3 shows rate measurement data for both respiration and heartbeat, with the receiver output at a null point. At the null point during continuous breathing, the Doppler measured "heart rate" is actually the difference between the real heart rate and respiration rate values. The measured "respiration rate" is actually twice the real value [19].

Droitcour et al. proposed to avoid these null detection points with a quadrature receiver, where two receiver chains with LO phases 90° apart insure that there is always at least one output not in the null detection point [30]. The two output channels of a quadrature receiver will be

$$\begin{cases} B_I(t) = \cos\left(\theta + \dfrac{\pi}{4} + \dfrac{4\pi x(t)}{\lambda} + \Delta\Phi\right) \\[2mm] B_Q(t) = \cos\left(\theta - \dfrac{\pi}{4} + \dfrac{4\pi x(t)}{\lambda} + \Delta\Phi\right). \end{cases} \tag{5}$$

When $\theta + \pi/4$ is an even/odd multiple of $\pi/2$, the I channel signal will be at the null/optimum detection point while the Q

channel signal will be at the optimum/null detection point. In these cases, there will always be one channel at the optimum detection point to guarantee good detection accuracy. With a quadrature receiver, the worst case is when θ is an integer multiple of π so both $\theta + \pi/4$ and $\theta - \pi/4$ are odd multiples of $\pi/4$, and neither receiver chain is at the optimum phase-demodulation point. The baseband outputs at this point are

$$\begin{aligned} B_I(t) &= B_Q(t) \\ &\approx \frac{1}{\sqrt{2}} - \frac{1}{\sqrt{2}} \\ &\times \left[\left(\frac{4\pi x(t)}{\lambda} + \Delta\Phi\right) + \frac{1}{2}\left(\frac{4\pi x(t)}{\lambda} + \Delta\Phi\right)^2\right]. \end{aligned} \tag{6}$$

As long as $x(t)$ is much less than λ, the linear term is much larger than the squared term carrying the movement information $x(t)$. Therefore, the fundamental of $x(t)$ will dominate and the motion information can still be detected. Furthermore, it is shown in [39] that when complex signal demodulation is used to combine the I and the Q channel outputs, robust automatic detection can be achieved without the requirement of selecting between the I/Q channels.

When small wavelength is used such that $x(t)$ is comparable to λ, a series of harmonic frequency tones will be produced. For a single-tone periodic movement, $x(t) = m\sin\omega t$ where m is the movement amplitude, $\omega = 2\pi f_m$ describes the movement frequency; for a more complex movement, it can be decomposed into a series of single-tone movements. Using Fourier series to expand the baseband signal $B(t)$, it can be expressed as [40]

$$\begin{aligned} B(t) &= 2\cdot\sum_{k=1}^{\infty} J_{2k}\left(\frac{4\pi m}{\lambda}\right)\cdot\cos 2k\omega t\cdot\cos\Phi \\ &- 2\cdot\sum_{k=0}^{\infty} J_{2k+1}\left(\frac{4\pi m}{\lambda}\right)\cdot\sin(2k+1)\omega t\cdot\sin\Phi \end{aligned} \tag{7}$$

where $\Phi = \theta + \Delta\Phi(t)$ is the total residual phase, and $J_n(x)$ is the nth-order Bessel function of the first kind. Note that the term $J_0(4\pi m/\lambda)\cos\phi$ is neglected in the above equation since it is dc term. Therefore, the phase-modulated baseband signal is decomposed into a number of harmonics of the fundamental frequency. While the movement frequency ω is readily obtained from the fundamental frequency of $B(t)$, the above equation also shows that for a certain carrier frequency, the relative strength among the harmonics is decided by the movement amplitude m and the residual phase Φ. For example, the absolute value of ratio among the first-, second-, third-, and fourth-order harmonics is

$$\begin{aligned} H_1 &: H_2 : H_3 : H_4 \\ &= \left|J_1\left(\frac{4\pi m}{\lambda}\right)\cos\Phi\right| : \left|J_2\left(\frac{4\pi m}{\lambda}\right)\sin\Phi\right| : \\ &\quad \left|J_3\left(\frac{4\pi m}{\lambda}\right)\cos\Phi\right| : \left|J_4\left(\frac{4\pi m}{\lambda}\right)\sin\Phi\right|. \end{aligned} \tag{8}$$

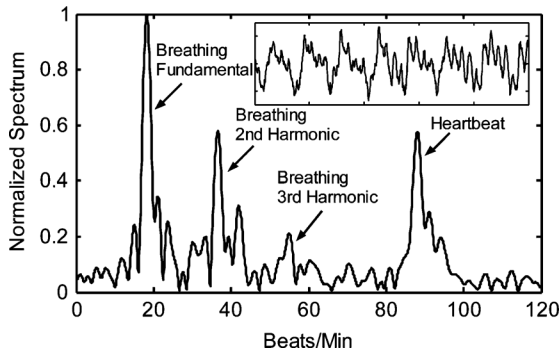Fig. 4 shows an example of the baseband spectrum detected using a carrier frequency of around 24 GHz. The second- and

Fig. 4.   Normalized baseband spectrum detected by a 24-GHz radar. (Inset: 27-s real time signal.) From [40].

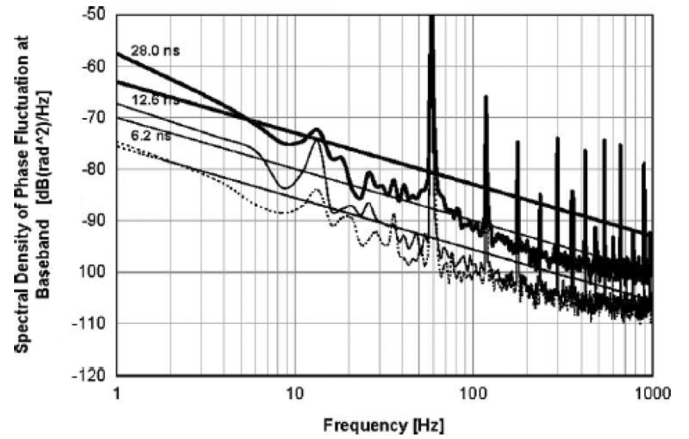

Fig. 5.   Measured and predicted spectral density of phase fluctuation at baseband for time delays of 28.0, 12.6, and 6.2 ns. From [30].

third-order harmonic of the breathing signal can be easily identified from the spectrum.

C. Range Correlation

As discussed in Section II, a CW radar typically transmits a single-tone signal and the received signal can be approximated by (1). The information about the periodic target motion can be demodulated if this signal is multiplied by an LO signal that is derived from the same source as the transmitted signal. This radar topology takes advantage of the ability to use the same oscillator for the transmitter and LO, which keeps the phase noise of the two signals correlated.

One of the challenges involved in using a silicon CMOS radar is the translation of oscillator phase noise, notoriously high in fully integrated CMOS oscillators, to output amplitude noise. When the same source is used for transmitting and receiving, the phase noise of the received signal is correlated with that of the LO, with the level of correlation dependent on the time delay between the two signals. For example, at a 50-cm range, the baseband noise at 10 Hz is 134 dB below the RF phase noise [29]. In a radar application, this time delay is proportional to the target range. When the delay is small, this effect greatly decreases the noise spectrum at baseband. Hence, this phase-noise-reducing effect is known as range correlation [41]. Range correlation is particularly important in measuring chest-wall movement since the heart and respiration information is encoded in phase modulations of 0.1–10 Hz, where the phase noise is very high [29].

Experiments have been carried out to verify the range-correlation effect [30]. The predicted and measured phase fluctuation spectral density are plotted in Fig. 5 for delays of 6.2, 12.6, and 28.0 ns, and offset frequencies from 1 Hz to 1 kHz. On average, the measured values were within 5 dB of the predicted values. The baseband phase noise was reduced from 148 to 136 dB at 1 Hz for the time delays from 6.2 to 28.0 ns, which correspond to ranges from 0.93 to 4.2 m [30]. The measured baseband noise spectral density was in the same range as predicted based on the previously measured phase noise and range-correlation theory. The measured baseband noise increased as the time delay increased and had approximately a 10-dB/decade slope, as was predicted.

In this experimental verification, the measured baseband noise spectrum agreed with theoretical values within an average of 5 dB. Free-running CMOS oscillators with -60 dBc $\cdot$ Hz

phase noise at a 10-kHz offset were found to be adequate for heart-rate detection at distances up to 50 cm. The use of a quadrature receiver improved the lowest accuracy, which occured at the phase-demodulation null point, from 40% to 80%.

III. RF FRONT-END ARCHITECTURES

The front-end architecture plays an important role in maximizing the sensitivity, extending the detection range, and rejecting interferences. Various RF front-end architectures have been reported. In addition to previously used homodyne, heterodyne, and double-sideband architectures, direct IF sampling and self-injection locking were recently proposed. The properties of these front-end architectures will be discussed in this section.

Fig. 6.   Simplified block diagram of a homodyne motion detector.

A. Homodyne

To eliminate the null detection problem of a single-channel Doppler radar, quadrature radar architecture can be used for homodyne architecture. A simplified block diagram of homodyne motion detector is shown in Fig. 6. Since there are in-phase and quadrature (I/Q) baseband outputs, there is always one channel not at the null detection point. Moreover, since the vital sign signal has low bandwidth, the two output channels can be combined in software to perform complex signal demodulation [22] or AT demodulation [19] as low-cost baseband solutions, which will be discussed in Section IV.

B. Heterodyne

Heterodyne radio architecture [4], [5] has been the only solution for noncontact vital sign detection until the homodyne

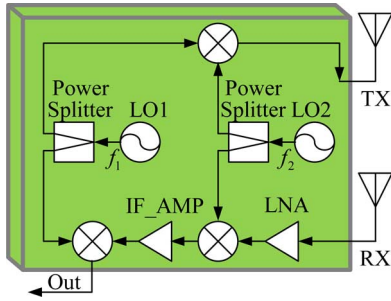Fig. 7. Double-sideband architecture for vital sign detection radar.

Fig. 8. Direct IF sampling architecture.

noncontact vital sign detector was first demonstrated at the beginning of this century [29], [42]. Compared with the homodyne architecture, the heterodyne architecture has the advantage of robustness against dc offset. However, single-channel heterodyne radar has the null detection point problem. In order to overcome the null detection point problem, quadrature architecture or frequency tuning on a single channel has to be used. In 2005, a double-sideband transmission heterodyne architecture was proposed to eliminate the need for generating quadrature LO and several filtering requirements in traditional heterodyne architecture [43].

C. Double Sideband

The double-sideband architecture for vital sign radar is a type of heterodyne architecture without image band rejection. After mixing RF LO and IF LO, both upper sideband (USB) and lower sideband (LSB) are transmitted, and the radar receives and down-converts the reflected signals of both sidebands by mixing them with the same RF LO and the same IF LO. Thus, the vital sign signals modulating on both USB and LSB, respectively, are automatically combined in baseband. Fig. 7 shows an example of this architecture. It is useful when designing vital sign radars operating at high frequencies such as millimeter wave or above. It eliminates the need of generating accurate quadrature RF LO for homodyne architecture or using image rejection filters for heterodyne architecture at high frequencies. The usefulness was accidentally discovered when building a Ka-band radar for vital sign detection [43]. Without quadrature I and Q outputs, the radar worked robustly without null detection point issue. Since the USB and LSB have different wavelengths, the null detection points for USB and LSB are not collocated until every 1/8 of the IF wavelength, which can be designed to be fairly large. By adjusting the IF frequency, the locations of overlapping USB and LSB null points can also be moved, giving the robustness of this architecture [44].

The double-sideband architecture provides an advantage when it comes to monolithic integration. Without the need of image rejection filters and quadrature generation, the radar transceiver can be easily designed and integrated on a semiconductor chip. A 5-GHz double-sideband vital sign detection radar chip has been fabricated using a UMC 0.18-μm CMOS process [32]. The chip fully integrates all building blocks in the RF transceiver and has simple I/O of TX output, RX input, and baseband output. Note that an analog-to-digital converter (ADC) can potentially be integrated to provide digital output.
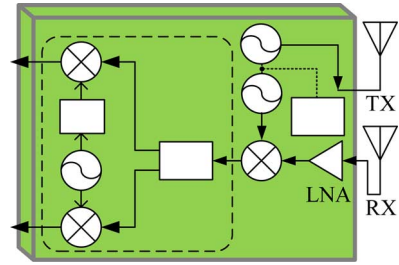
D. Direct IF Sampling

For the conventional quadrature direct-conversion architecture, I/Q imbalance and dc offset are two inevitable challenges that degrade the demodulation accuracy and the output signal-to-noise ratio (SNR). To ensure I/Q amplitude and phase balance, complicated calibration procedures have to be applied [45]. By using a digital I/Q demodulation technique, the two output channels are in a perfect quadrature phase relationship, making calibration procedures unnecessary. To overcome the dc-offset problem, subsystems such as the dc offset compensation unit [19] are needed. However, these methods add to the system complexity and increase the hardware cost. If configured with a heterodyne architecture, there will be no significant amount of dc offset. Therefore, direct IF sampling with a heterodyne architecture has been proposed for noncontact vital sign detection [46]. Fig. 8 shows the block diagram of direct IF sampling architecture. In the receiver chain, the mixer after LNA down-converts the received signal into an IF. A high-speed ADC is then used to convert the analog IF signal to digital. After that, quadrature demodulation is performed using a high-speed digital signal processor (DSP).

Extensive experimental verifications have been carried out in [28] to demonstrate the direct IF sampling architecture's advantages in alleviating I/Q imbalance and eliminating the complicated dc-offset calibration. Since the information bandwidth of vital sign signals is very small, IF can be chosen at a low frequency such that the demand on ADC sampling speed can be relaxed. Therefore, this architecture is suitable for integrated circuit implementation. Moreover, the architecture can be developed into a low-IF radar sensor with potential benefits of higher detection sensitivity [47].

IV. BASEBAND SIGNAL PROCESSING METHODS

The challenges for baseband signal processing include the demodulation of the baseband signal, the removal of undesired motion noise, and the isolation of the desired signal from multiple subjects. Many research activities are being conducted to solve the challenges, resulting in advanced baseband signal processing methods. Some of them are discussed in this section.

A. AT Demodulation

One way to eliminate the optimum/null detection point problem in the quadrature demodulation system is to use AT demodulation by calculating the total Doppler phase shift as $\Psi = \arctan[Q(t)/I(t)]$. Since Ψ is directly proportional to the
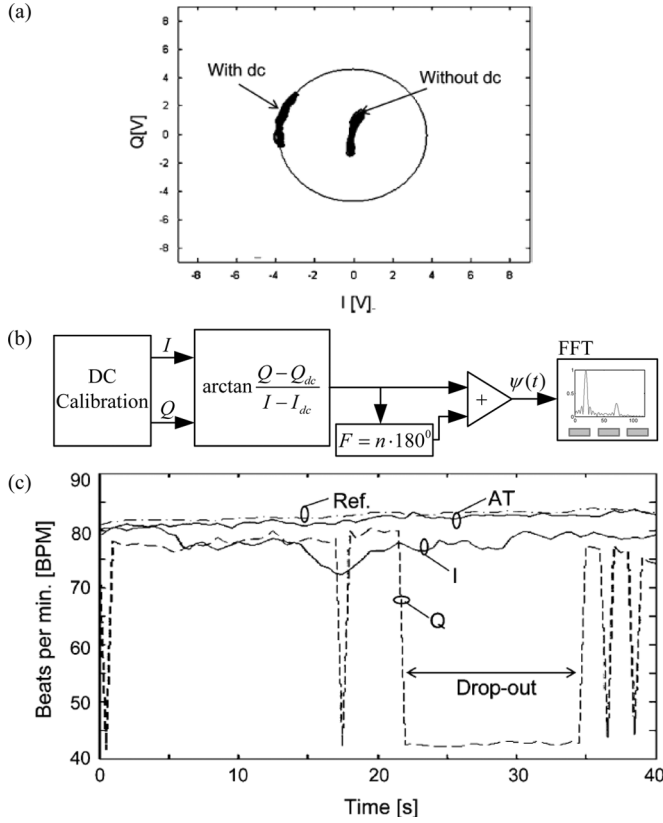
(a)

(b)

(c)

Fig. 9. (a) Constellation graph of I/Q data with/without dc information preserved and (b) block diagram for AT demodulation. The advantage of AT I/Q demodulation over I or Q is shown in (c) for a measurement of heart rate where Q is at a null, compared against a wired finger pulse sensor. From [19].

movement $x(t)$, desired motion information can be recovered reliably.

Two important issues determine the performance of AT demodulation. First, the radar receiver suffers from dc offset at the RF front-end output, which is caused by circuit imperfection and the reflections from stationary objects (clutter) surrounding the body. This will directly lead to demodulation error in $\arctan[Q(t)/I(t)]$. Second, since 180° phase discontinuity happens in the AT function when the signal trajectory crosses the boundary of two adjacent quadrants, an effective phase unwrapping algorithm is necessary to recover the correct motion information. Therefore, the AT demodulation algorithm is formulated as

$$\psi(t) = \arctan\frac{Q(t) - Q_{\mathrm{dc}}}{I(t) - I_{\mathrm{dc}}} + F = \frac{4\pi x(t)}{\lambda} + \Delta\Phi \quad (9)$$

where F is a multiple of 180° for the purpose of eliminating the discontinuity when $\psi(t)$ crosses the boundary of two adjacent quadrants in the constellation graph, Q_{dc} and I_{dc} are the total undesired dc offset generated by electronic circuit and clutter reflection. Fig. 9(a) shows the constellation graph of the I/Q data with/without dc information preserved. Fig. 9(b) shows the block diagram for AT demodulation.

An illustration of the performance benefit in an AT I/Q demodulated heart rate measurement is shown in Fig. 9(c). I, Q, and AT demodulated signals were measured for a position where the Q channel was close to a null condition. The radar-measured
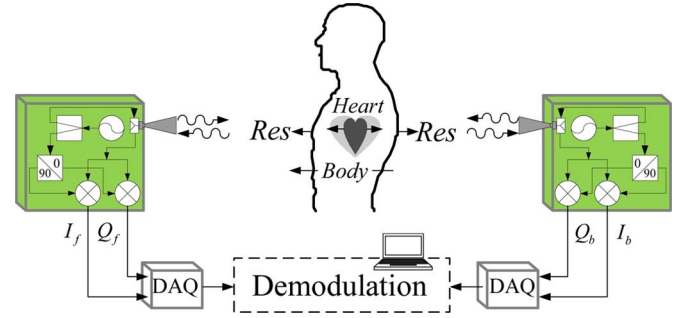

Fig. 10. Setup of random body motion noise cancellation by detecting from two sides of a human body. From [22].

heart rate was compared with the reference (Ref.) heart rate obtained from a wired finger pressure pulse sensor (UFI1010). The Q channel rate shows dropout regions (in 35% of the interval) when the SNR is insufficient for digitization, as occurs with the squaring effect due to the null position. Excluding dropouts, the I and Q channels have errors of 4.8 or 5.2 beats, respectively, over the same 40-s interval where the AT data has an error of only 0.9 beats.

B. Body Motion Noise Reduction

Since noncontact vital sign detection is based on sensing small physiological movements in the millimeter or centimeter range, the presence of random body movement produces a significant source of noise for accurate detection. Although successful Doppler radar noncontact vital sign detection under different environments for different applications has been reported, a critical issue that prevents this technology from being widely used is the noise produced by random body movement. For example, when the radar is used for overnight monitoring of sleep apnea, the detected signal will be interrupted when the subject under test rolls over on the bed, producing false alarm.

To overcome the challenge of random body motion noise, multiple transceivers have been used to cancel the noise caused by motion artifacts such as random body motion. It has been demonstrated that based on the different movement patterns of physiological movement and random body motion, it is possible to cancel out the noise caused by random body movement using multiple transceivers detecting from different sides of a human body [39], [48]. Fig. 10 shows an example of the noise cancellation setup, where two antennas are used to detect from the front and the back of a human body simultaneously. When generating the desired physiological signal, the expansion and contraction of heart and chest have the same movement direction relative to each antenna. However, when the body is randomly roaming toward one radar, it is moving away from the other. Based on this difference, the noise caused by random body motion was significantly reduced by multiplying the signal detected from both sides. Extension to 2-D body motion noise cancellation was also reported with four radar sensors detecting from four sides of a human body [48].

Another solution to improve the performance against random body motion is the differential front-end Doppler radar operating at two different frequencies. By using dual helical antennas each with a 40° beamwidth, it is possible to illuminate

the body in two adjacent locations to perform a differential measurement. Since only one of the beams illuminates the heart, the baseband signal from the second radar is used for motion cancellation. A dual helical antenna and simple direct-conversion radar were implemented to demonstrate this approach [23].

Similar approaches such as two-frequency radar sensor [24] and multi-frequency interferometric radar [25] have also been reported recently. Combined with advanced signal processing, these technologies can improve the performance of noncontact vital sign detection. Signal processing standalone methods include the use of empirical mode decomposition, which can break the radar signal down into its components and help separate and remove fidgeting interference, even when the interference falls near the same frequency as the cardiopulmonary motion [49]. This method is also suitable for shake cancellation in handheld radar, as is the use of radar mounted accelerometers when isolating subject motion from radar motion [50].

C. Detection of Multiple Subjects

It was found in experiments that other major problems of Doppler non-contact motion detection include the noise caused by other motion artifacts and the presence of multiple subjects. A multiple-input multiple-output (MIMO) technique was then proposed to solve the problems. Another proposed approach is the single-input multiple-output (SIMO) technique. In [51]–[54], the single and multiple antenna systems and SIMO/MIMO signal processing were explored to isolate desired radar return signals from multiple subjects. A generalized likelihood ratio test (GLRT), based on a model of the heartbeat, has been developed to show that this technique can be used to distinguish between the presence of 2, 1, or 0 subjects, even with a single antenna. Furthermore, this technique was extended to detect up to $2N - 1$ subjects using N antennas.

To demonstrate the use of GLRT to separate multiple subjects, three different sets of measurements with a single antenna were carried out. The measurements were at first filtered with a 0.8–2-Hz bandpass filter to remove respiration and higher order harmonics. They were then divided into overlapping intervals of length of 15 s. The test statistic was evaluated in each interval. The results in Fig. 11 show that it is objectively possible to determine the number of persons based on the test statistic, e.g., by using threshold of 1.25. It should be noted that once it has been determined that less than two persons are present with the above test, another GLRT can then be used to distinguish zero and one person.

V. OTHER RECENT DEVELOPMENTS

A. CMOS/BiCMOS Radar-on-Chip Integration

In the early 2000s, researchers in Bell Labs used direct-conversion quadrature receiver architecture to successfully integrate the radar's RF front end in a small chip [29], [30], [42], [55], which is compact, lightweight, and inexpensively mass producible. It set an important milestone in history on research of detecting subject's heartbeat and respiration using electromagnetic waves. Fig. 12 shows the photograph of the first chip, which was implemented in a 0.25-μm CMOS process. The chip
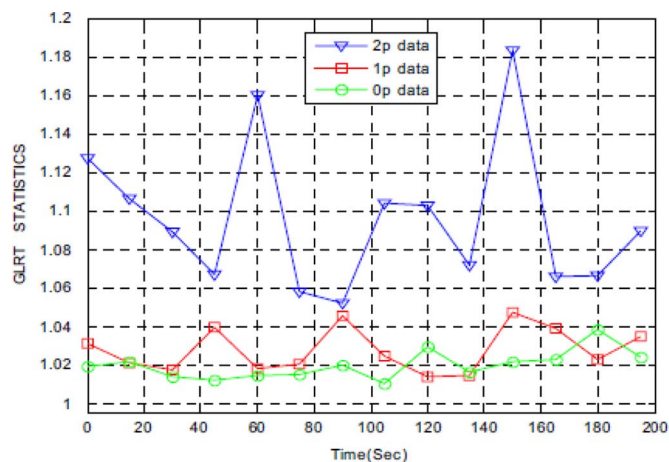
Fig. 11.   GLRT test statistics when two persons, one person, or zero person was detected by a single antenna. From [51].
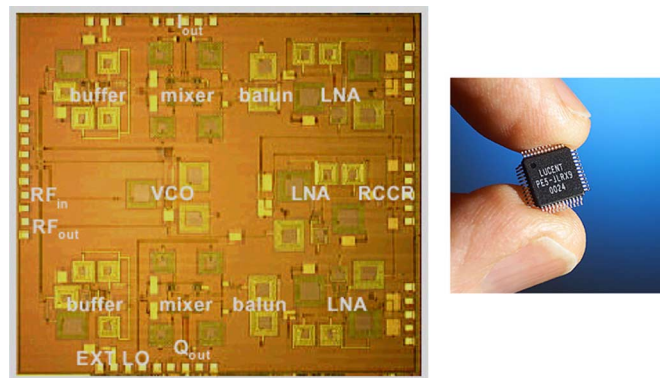
Fig. 12.   First noncontact physiological motion sensor chip using quadrature receiver architecture. From [29].

was packaged in a TQFP 48-pin package. It delivered 2 mW at RF output and dissipated 180 mW from dc supply [55].

The first generation of on-chip biomedical radars operated at 1.6 and 2.4 GHz, each with a single oscillator and output power comparable to the low-end power of consumer electronics (under 10 mW). The 2.4-GHz radar used a quadrature I/Q receiver in order to avoid null points [30], and thus, improved upon the accuracy of 1.6-GHz radars described in [42] and [29].

Following the demonstration of the first noncontact physiological motion sensor chip, several other CMOS radar-on-chip implementations have been demonstrated for noncontact vital sign detection. Fig. 13(a) shows a double-sideband chip designed with a double-sideband architecture in 0.18-μm process [32]. It integrated all the RF building blocks so that the transmitter output can be directly transmitted to a target and the receiver output can be directly processed by baseband circuits. Fig. 13(b) shows a high-sensitivity receiver chip in a 0.13-μm process that is software configurable to set the operation point and detection range for optimal performance. All the analog functions are integrated on-chip so that the output can be directly sampled for digital signal processing.

Operating the vital sign detection radar at millimeter-wave frequency and above presents a challenge for detecting both respiration and heartbeat. This is because the respiration displace-

Fig. 13. Chip microphotograph of: (a) a double-sideband vital sign detection radar fabricated in 0.18-μm CMOS process and (b) a direct conversion radar fabricated in 0.13-μm CMOS process. From [31] and [32].

Fig. 14. 60-GHz micro-radar. (a) System block diagram. (b) Photograph of the integrated radar. From [56].

Fig. 15. Doppler radar respiratory monitoring using harmonic tag attached to the subject to reject undesired interference from other objects. From [57].

10 g. The total power consumption of RF, IF, and baseband circuits is 377 mW from a 1.2-V supply. The 60-GHz micro-radar can detect vibrations as small as 20 μm from 0.3 m away and can certainly detect respiration displacement, as well as heartbeat while the subject is holding the breath. The challenge arises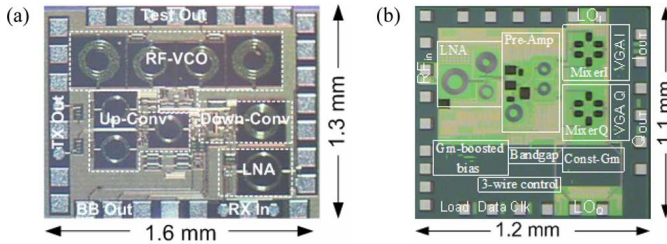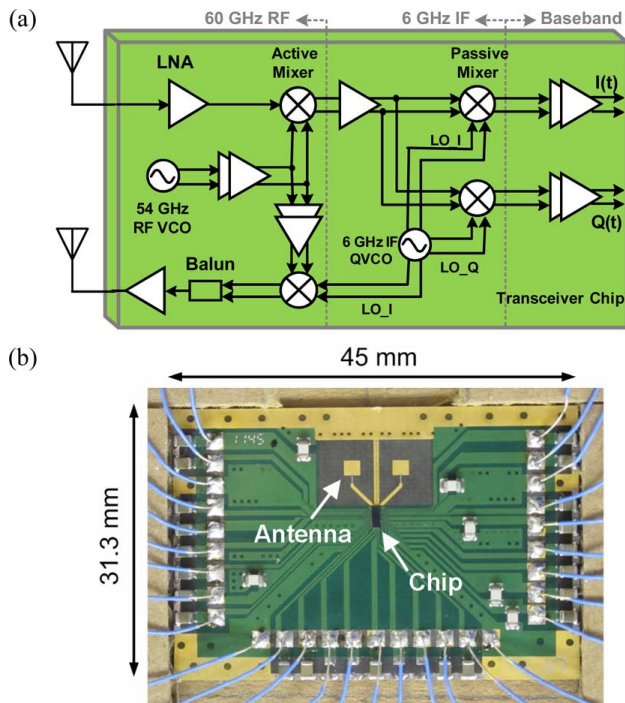 when trying to detect both respiration and heartbeat because the large respiration displacement introduces strong nonlinear phase modulation effect that interferes with the detection of small heartbeat displacement. A further signal processing technique is in need to solve this issue.

B. Passive Harmonic Tag

Harmonic tags can be used to isolate desired targets from clutter in Doppler radar systems. A system that can isolate small motion of a tagged target in the presence of motion of untagged objects would provide a means for improved SNR for isolating cardiopulmonary motion from other body motion. A harmonic tag consists of a tag antenna with a strongly nonlinear element, normally realized by a Schottky barrier diode. Fig. 15 shows an experimental setup using a passive harmonic tag to isolate the desired vital sign signal with undesired signals [57]. The incoming signal to the harmonic tag is converted to its second-order harmonic by the nonlinear element, and the tag is designed such that the second harmonic is transmitted back to the receiver. By detecting the reflected signal at the second-order harmonic frequency of the transmitted signal, the radar rejects interference and noises reflected from other objects based on frequency discrimination.

Fig. 16 shows that harmonic Doppler radar was able to detect and track respiration rate that corresponds to moving tag on the chest of a human subject even in the presence of large moving reflecting object. In this experiment, the radar transmit power was 10 dBm. A large moving reflecting object was placed near the subject under test. A contact monitor was used to provide a reference of the respiration rate. The noncontact radar was able to track the respiration rate with a maximum error of less than 0.5 BPM. Heterodyne methods have demonstrated advantage over homodyne methods in such systems [27].

RF tags can also be used to isolate nontagged motion when in the presence of tagged motion. This can be useful for detecting

ment is comparable to the wavelength and the heartbeat displacement is usually much smaller. In this case, the harmonics of respiration signal due to nonlinear modulation in (7) complicates the spectrum, and the sensitivity may no longer increase with decrease in wavelength [33]. Nevertheless, the small size of the antenna and the potential of vital sign imaging using a phased-array technique still draws interest. By using a UMC 90-nm CMOS process and flip-chip packaging to integrate with the antennas, a system-in-package micro-radar for vital sign detection was recently demonstrated [56]. The micro-radar operates at a 60-GHz unlicensed band and uses a heterodyne architecture with quadrature demodulation at IF = 6 GHz. Although the propagation of 60-GHz signal in air experiences high loss due to oxygen absorption, this unlicensed band is suitable for short-range vital sign detection.

The system architecture of the radar transceiver chip is shown in Fig. 14. A picture of the micro-radar indicating the locations of the radar transceiver chip and the antennas is also shown. The complete micro-radar hardware is small and weighs less than
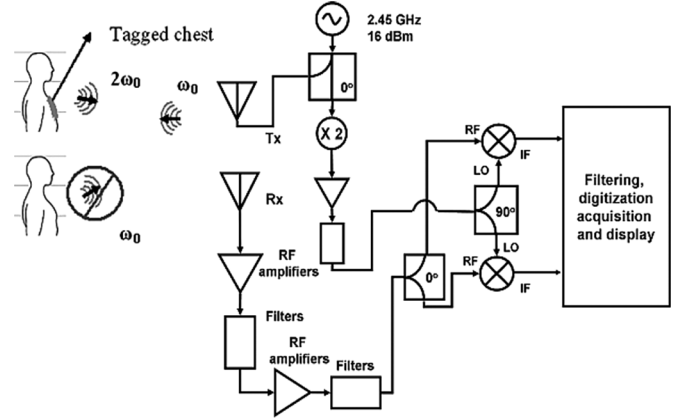
Fig. 16. Respiration rate of a human subject in the presence of a large moving object. The maximum error did not exceed 0.5 BPM. From [57].

Fig. 17. Block diagram of dc-coupled displacement radar. From [14].

Fig. 18. (a) Constellation graph and (b) target movement detected by ac- and dc-coupled radar. From [14].

the presence of a victim near a rescuer. The physiological motion from the rescuer appears as noise when one is attempting to identify the physiological motion of the victim with a conventional fundamental radar. If the rescuer is wearing a harmonic tag, an additional harmonic radar can be used to isolate the motion of the rescuer, and this data can be used to create a filter for this data within the fundamental radar system, leaving only the victim's motion signal [58].

C. DC-Coupled Displacement Radar

In CW radar measurement, the radar sensor suffers from dc offset at the down-converter output, which is mainly caused by the reflections from stationary objects surrounding the target. The dc offset may saturate or limit the dynamic range of the following stages of baseband amplifiers. To overcome this limitation, ac coupling is commonly used in radar sensors. However, due to the high-pass characteristics of the coupling capacitor, ac coupling leads to significant signal distortion when the target motion has a very low frequency or a dc component. Physiological signal either changes with a low speed or tends to be stationary for a period. This creates a significant problem in vital sign detection using CW radar. To deal with this issue, several approaches, such as high RF-LO isolation mixers [21], have been developed to employ dc coupling in radar sensors. However, these approaches are either cumbersome to implement or do not completely remove dc offsets and limit the dynamic range of the baseband amplifiers.

Recently, an adaptive dc-coupled CW radar sensor with feedback loops enabled by RF coarse tuning and baseband fine tuning is proposed. The block diagram of the implemented dc-coupled CW radar is shown in Fig. 17. The RF tuning is implemented using a path of an attenuator and a phase shifter at the RF front end of the radar sensor [59], [60]. This approach adds a portion of the transmitter signal to the receiver input to cancel out most of the dc offset. To further calibrate the remaining dc offset, the baseband fine-tuning architecture will be used to adaptively adjust the amplifier bias to the desired level that allows both high gain and the maximum dynamic range at the baseband stage. With the above-mentioned dc tuning architectures, the radar sensor will be able to measure low-frequency motions and even stationary moment. The adaptive feedback architecture will allow the radar sensor to work

with the largest dynamic range and be able to detect movement with stationary moment.

Experiments have been carried out to demonstrate the advantage of dc-coupled radar. During experiment, an actuator controlled by a computer was used to generate a motion pattern that was monitored by both ac-coupled radar and dc-coupled radar. Fig. 18 shows the trajectory of the baseband outputs, where the trajectory of the dc-coupled radar matches well with the unit circle, while the ac-coupled radar tends to deviate from the circular arc to form a ribbon-like shape. This is because of the variation of radar signal amplitude that is caused by the ac coupling capacitors' charging and discharging. Since the dc-coupled radar has a trajectory that is much closer to an ideal arc, it can be used for a more accurate dc calibration, and therefore leads to more accurate AT demodulation. To verify the dc-coupled radar's ability to preserve the dc information of stationary moment, both the dc radar and ac radar were used to measure the

actuator move close to a sinusoidal pattern, but with a stationary moment after each cycle. The measurement results were shown in Fig. 18(b). It is seen that the dc-coupled radar successfully preserved the stationary information and precisely matched with the programmed actuator motion. However, the ac radar measured movement starts to deviate from the ground truth when the stationary moment begins.

Therefore, the proposed dc-coupled radar sensor is expected to precisely measure the respiration motion pattern that has a very low frequency and a short stationary moment after each cycle. An application example of the dc-coupled radar is tumor tracking for lung cancer radiotherapy [14], [15], where precise information of tumor displacement is desirable during radiotherapy to improve the efficacy and minimize damage to surrounding healthy tissues.

D. Self- and Mutual-Injection Locking

Self-injection locking was first demonstrated by Wang *et al.* [61] as a technique that can be used in Doppler radar to detect vital signs. The technique originated from the authors' previous work on spectrum sensing using injection locking [62]. Instead of detecting wireless signals in the air through injection locking that locks the free-running voltage-controlled oscillator (VCO), the VCO can transmit its signal through an antenna and use the reflected signal from a target to lock itself. If the target is moving, the frequency or phase of the reflected signal will be modulated due to the Doppler effect. After self-injection locking, the VCO's frequency or phase will carry the Doppler modulation due to the target's motion. The motion signals, such as vital signs, can then be extracted through frequency demodulation. The concept and architecture is illustrated in Fig. 19(a). Detailed theoretical analysis involving the self-injection locking and frequency demodulation can be found in [61] and [63]. Using this technique and two self-injection locking radars similar to the body motion noise cancellation technique [22], as shown in Fig. 19(b), vital signs of a subject jogging on a treadmill were successfully detected. The two radars are mutually locked because the transmitted signal from each radar injects into the other radar. The baseband signal can then be collected and processed from either radar [64]. This is believed to be the first demonstration of noncontact vital sign detection of a subject jogging on a treadmill.

VI. Clinical Validations

A. Experiment on an Infant Simulator

Infant simulators [65]–[67] can mimic cardiovascular derangements seen in critically ill infants. In the Neonatal Intensive Care Unit (NICU), Shands Hospital, University of Florida, Gainesville, FL, USA, preliminary experiments have been performed with infant simulators to demonstrate the efficacy of noncontact vital sign detection radar in children and baby healthcare [68]. A 5.8-GHz homodyne Doppler radar was placed underneath the crib where radio waves can penetrate through a nonmetal structure to reach the infant simulator. The experiment was conducted through 18 continuous events. In each event, respiratory rate (RR), heart rate (HR), and tidal volume (TV) were controlled and changed by software.
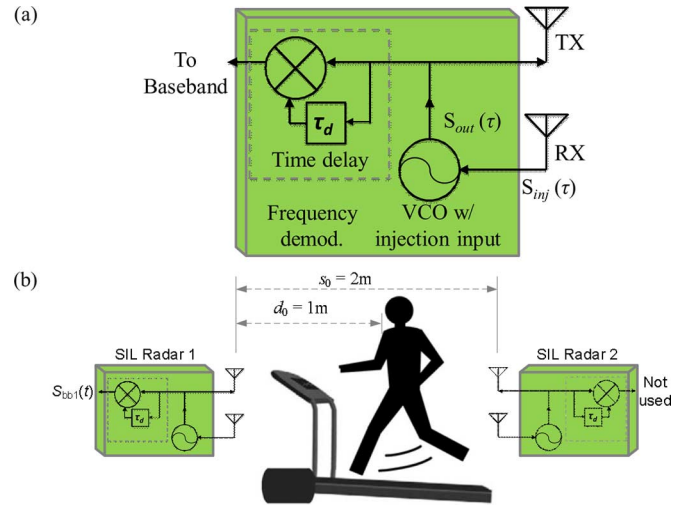

Fig. 19. (a) Self-injection-locking technique for vital sign detection. (b) Detecting vital signs of a subject jogging on a treadmill using two mutually injection-locked self-injection-locking radars. From [62] and [64].
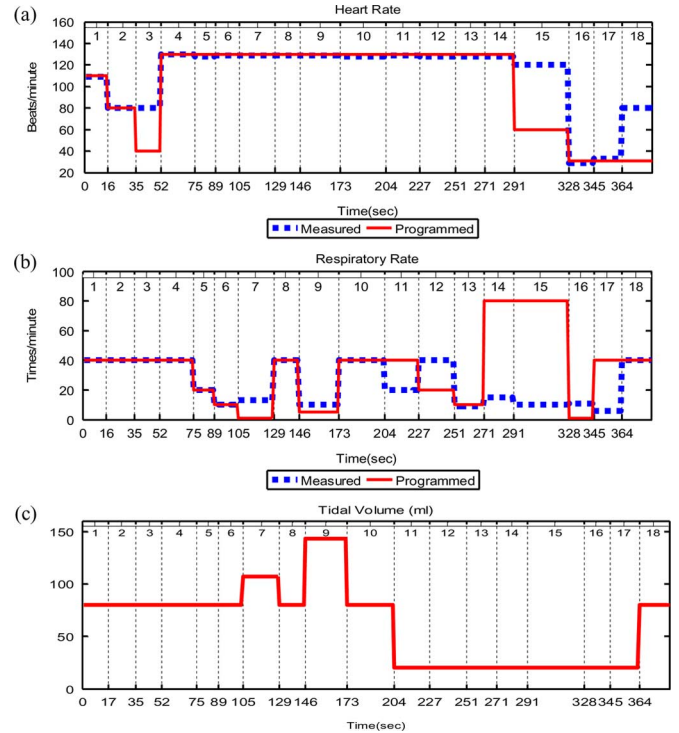

Fig. 20. (a) Heart rate, (b) respiratory rate, and tidal volume (TV) recorded during experiment on infant simulator. From [68].

Fig. 20(a) and (b) shows the measurement results and programmed values of heart rate and respiratory rate of typical clinical ill syndromes such as tachypnea (Events 14 and 15) and bradypnea (Events 7 and 9) and other special cases. Fig. 20(c) is the programmed respiratory tidal volume of each event. Bigger TV indicates larger amplitude of respiration. When TV drops to 20 mL, the breathing becomes very weak.

The experimental results proved that the radar sensor can achieve accurate detection results when the infant simulator was in a baseline or normal physiologic state. Although the results have deviation to the programmed values when detecting the

infant under abnormal conditions, they can reflect the change of vital signs under abnormal conditions and provide approximate data that are useful for initial diagnose of specific syndromes. Detailed analyses of the typical cases were presented in [68]. Analysis also suggested possible techniques for further improvement, such as direct coupling circuit, carrier frequency tuning, and more sophisticated spectral analysis.

B. Human Studies

The efficacy of Doppler radar as a substitute for conventional respiratory monitors has been demonstrated in human population studies. Testing conducted using a spirometer, which is an apparatus for measuring the volume of air inspired and expired by the lungs simultaneously with Doppler radar have indicated that displacement-based tidal volume measurements are possible with the subject in a known position [11]. A short-term measurement on ten awake supine subjects was carried out, where tidal volume was obtained using a 2.4-GHz quadrature Doppler radar system, and compared with a spirometer. The study indicated that it was possible to establish a correlation parameter between chest displacement and tidal volume for each subject. A Bland-Altman plot for spirometer versus radar TV measurements is shown in Fig. 21(a). In this graphical method, the difference between the two techniques (bias) is plotted against the averages of the two techniques. Horizontal lines are drawn at the mean difference, and at the limits of agreement, which are defined as the mean difference plus and minus 1.96 times the standard deviation of the differences. When the data falls between these limits, each of the two methods can be considered an equivalent substitute for the other, as is the case here.

In another study [12], clinical results were obtained validating the accuracy of respiratory rate obtained for hospitalized patients using a noncontact low-power 2.4-GHz Doppler radar system. Twenty-four patients were measured, and the respiratory rate accuracy was benchmarked against the respiratory rate obtained using a Welch Allyn Propaq Encore model 242, the Embla Embletta chest-belt system, and by counting chest excursions. The 95% limits of agreement between the Doppler radar and reference measurements fell within ±5 breaths/min. A Bland-Altman plot comparing the radar and Embletta system appears in Fig. 21(b).

C. Assessment of Cardiopulmonary Effective RCS and Displacement

A technique for the precise assessment of key parameters relating to cardiopulmonary activity was proposed in [13]. A dual-band radar system operating at 2.4 and 5.8 GHz was developed for the experiment setup, which is shown in Fig. 22. Quantitative analyses of the return signal, in terms of intensity and phase modulation magnitude, were performed. Fig. 23 shows the center-tracked arcs for the subject in the supine, prone and side positions at the 2- and 1-m range with a 2.4-GHz carrier.

Based on the study carried out in [13], two parameters can be used to assess cardiopulmonary activity. The first parameter, defined as the cardiopulmonary effective radar cross section (ERCS), is a measure of the radar cross section of the portion of the torso surface that moves due to respiration and heart-
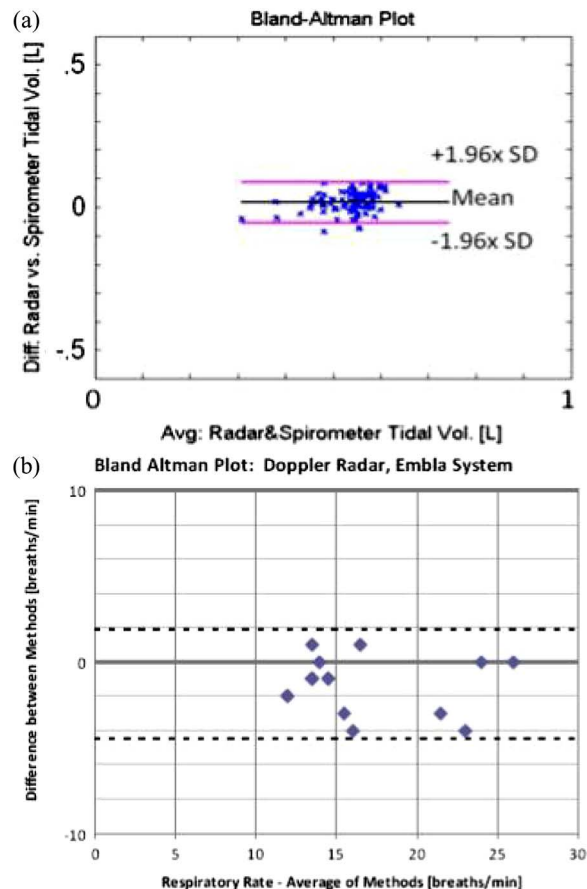

Fig. 21. Bland-Altman comparisons showing equivalence: (a) between spirometer and radar based tidal volume measurements and (b) between chest-belt and radar based respiratory rate systems. From [11] and [12].
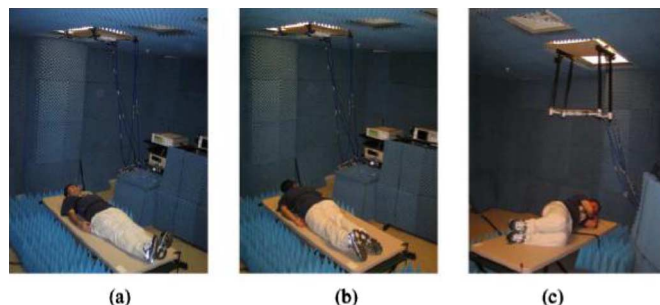

Fig. 22. Experiment setup for radar-based assessment of cardiopulmonary activities. The subject was lying in: (a) supine and (b) prone positions at the maximum measurements range, and in (c) side position at a short range. From [13].

beat activity. The second parameter corresponds to the maximum displacement of the torso surface in the direction of incidence. The dual frequency radar system was used to determine cardiopulmonary ERCS and displacement. A system calibration procedure using spherical targets was provided and displacement measurement was validated for the dual-frequency system. Preliminary testing results consistently showed an ERCS that is larger for the back of the torso and smaller for the side compared to the front, while the respiration depth is smaller in the prone position than in supine. Determination of body orientation is essential for displacement-based measurements like tidal volume [11]. With ERCS tracking, a radar system can automatically de-
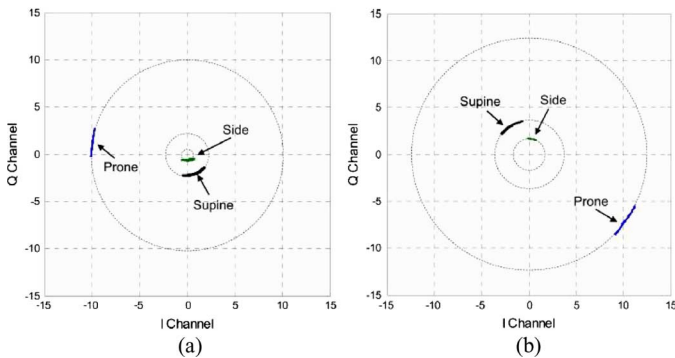
Fig. 23. Center-tracked arcs for the subject in the supine, prone, and side positions at 2-m range with 2.4-GHz carrier. The circle radius was: (a) 2.27, 10.06, 0.75 V at 2 m (b) and 3.58, 12.49, 1.67 V at 1 m when detecting from the front, back, and side, respectively. From [13].

termine orientations and therefore apply the correct calibration relating displacement to tidal volume.

VII. RELATED TECHNOLOGIES AND FUTURE TRENDS

Another important wireless solution for noncontact healthcare monitoring is the ultra-wideband (UWB) radar [69]–[72]. By controlling the delay between the inputs of the correlation function block inside a UWB radar, which corresponds to the signal round-trip traveling time, the detection range can be controlled. This mechanism makes it possible for UWB radar to eliminate interference caused by reflection from other objects and multi-path reflection. This is the main advantage of UWB vital sign detection radar. However, most of the UWB radars require the internal delay to be accurately calibrated, thus increasing the system complexity. In addition, since the correlation function may be nonlinear, it may be nontrivial for UWB radar to recover the original movement pattern even though frequency information can be easily obtained.

Compared to UWB radar, CW Doppler radar has the advantages of low power consumption, simple radio architecture, and ease of silicon integration. Moreover, it is easier for CW Doppler radar to extend the detection range. However, problems of clutter noise, micro-Doppler scattering from other parts of a body (e.g., arm and leg), and multiple-target identification are still under intensive research for pure CW Doppler radar.

Frequency-modulated continuous-wave (FM-CW) radar [73] is another technology that has shown potential for noncontact healthcare application. Being able to localize the target from a distance away [74], the FM-CW radar can further extend the application to patient and elderly care in smart houses and ambulatory environments, where the subjects could be very mobile.

Because UWB radar, CW Doppler radar, and FM-CW radar each has its own advantages and shortcomings, hybrid mode radars [75], [76] that integrate multiple mechanisms have recently drawn many research interests. It is expected that the advancement in the integration of hybrid detection mechanisms will result in higher performance of noncontact biomedical radar for healthcare applications.

VIII. CONCLUSION

Over the past few decades, there have been significant advancements in the development of Doppler radar sensors for noncontact healthcare monitoring. Various hardware architectures have been demonstrated from bench-top systems to CMOS/BiCMOS radar-on-chips. Whereas the hardware technologies are the key factors in realizing high detection sensitivity and large detection range, advanced signal processing methods are equally important to solve several challenges such as random body motion artifact and presence of multiple targets. While the radar sensor is sensitive enough to pick up tiny physiological movements due to breathing and heartbeat, it can also pick up any physical body movement or clutter noise. Therefore, advanced signal processing methods are still being investigated to make the radar robust enough to enter the life of ordinary people. On the other hand, smaller radar sensor with lower power consumption and higher detection sensitivity would likely be the focus of the hardware research. The efforts of many researchers who found this subject interesting and contributed to advances in technology development will hopefully bring the technology to wider use and benefit humanity in the future.

REFERENCES

[1] J. C. Lin, "Noninvasive microwave measurement of respiration," *Proc. IEEE*, vol. 63, no. 10, pp. 1530–1530, Oct. 1975.

[2] K.-M. Chen, D. Misra, H. Wang, H.-R. Chuang, and E. Postow, "An X-band microwave life-detection system," *IEEE Trans. Biomed. Eng.*, vol. BME-33, no. 7, pp. 697–701, Jul. 1986.

[3] H.-R. Chuang, Y. F. Chen, and K.-M. Chen, "Automatic clutter-canceler for microwave life-detection systems," *IEEE Trans. Instrum. Meas.*, vol. 40, no. 4, pp. 747–750, Aug. 1991.

[4] J. C. Lin, "Microwave sensing of physiological movement and volume change—A review," *Bioelectromagnetics*, vol. 13, pp. 557–565, 1992.

[5] K.-M. Chen, Y. Huang, J. Zhang, and A. Norman, "Microwave life-detection systems for searching human subjects under earthquake rubble or behind barrier," *IEEE Trans. Biomed. Eng.*, vol. 27, no. 1, pp. 105–114, Jan. 2000.

[6] J. Lin and C. Li, "Wireless non-contact detection of heartbeat and respiration using low-power microwave radar sensor," in *Asia–Pacific Microw. Conf.*, 2007, pp. 1–4.

[7] P. K. Capp, P. L. Pearl, and D. Lewin, "Pediatric sleep disorders," *Primary Care*, vol. 32, pp. 549–562, Jun. 2005.

[8] H. Forster, O. Ipsiroglu, R. Kerbl, and E. Paditz, "Sudden infant death and pediatric sleep disorders," *Wiener Klin. Wochenschrift*, vol. 115, pp. 847–849, Dec. 30, 2003.

[9] N. Hafner, I. Mostafanezhad, V. M. Lubecke, O. Boric-Lubecke, and A. Host-Madsen, "Non-contact cardiopulmonary sensing with a baby monitor," in *29th Annu. IEEE Int. Eng. Med. Biol. Soc. Conf.*, 2007, pp. 2300–2302.

[10] C. Li, J. Lin, and Y. Xiao, "Robust overnight monitoring of human vital signs by a non-contact respiration and heartbeat detector," in *28th Annu. IEEE Int. Eng. Med. Biol. Soc. Conf.*, 2006, pp. 2235–2238.

[11] W. Massagram, V. M. Lubecke, and O. Boric-Lubecke, "Microwave non-invasive sensing of respiratory tidal volume," in *Annu. IEEE Int. Eng. Med. Biol. Soc. Conf.*, 2009, pp. 4832–4835.

[12] A. D. Droitcour *et al.*, "Non-contact respiratory rate measurement validation for hospitalized patients," in *Annu. IEEE Int. Eng. Med. Biol. Soc. Conf.*, 2009, pp. 4812–4815.

[13] J. E. Kiriazi, O. Boric-Lubecke, and V. M. Lubecke, "Dual-frequency technique for assessment of cardiopulmonary effective RCS and displacement," *IEEE Sens. J.*, vol. 12, no. 3, pp. 574–582, Mar. 2012.

[14] C. Gu, R. Li, H. Zhang, A. Fung, C. Torres, S. Jiang, and C. Li, "Accurate respiration measurement using DC-coupled continuous-wave radar sensor for motion-adaptive cancer radiotherapy," *IEEE Trans. Biomed. Eng.*, vol. 59, no. 11, pp. 3117–3123, Nov. 2012.

[15] C. Li, C. Gu, R. Li, and S. B. Jiang, "Radar motion sensing for accurate tumor tracking in radiation therapy," in *12th Annu. IEEE Wireless Microw. Technol. Conf.*, Clearwater, FL, 2011, pp. 1–6.

[16] A. Singh, S. Lee, M. Butler, and V. M. Lubecke, "Activity monitoring and motion classification of the lizard Chamaeleo Jacksonii using multiple Doppler radars," in *Annu. IEEE Int. Eng. Med. Biol. Soc. Conf.*, 2012, pp. 4525–4528.

[17] A. Singh, N. Hafner, M. Butler, and V. M. Lubecke, "A data efficient method for characterization of chameleon tongue motion using Doppler radar," in *Annu. IEEE Int. Eng. Med. Biol. Soc. Conf.*, 2012, pp. 574–577.

[18] N. Hafner, J. Drazen, and V. Lubecke, "Fish heart rate monitoring by body-contact Doppler radar," *IEEE Sens. J.*, vol. 13, no. 1, pp. 408–414, Jan. 2012.

[19] B. K. Park, O. Boric-Lubecke, and V. M. Lubecke, "Arctangent demodulation with DC offset compensation in quadrature Doppler radar receiver systems," *IEEE Trans. Microw. Theory Tech.*, vol. 55, no. 5, pp. 1073–1079, May 2007.

[20] C. Gu and C. Li, "DC coupled CW radar sensor using fine-tuning adaptive feedback loop," *Electron. Lett.*, vol. 48, pp. 344–345, 2012.

[21] X. Zhao, C. Y. Song, V. Lubecke, and O. Boric-Lubecke, "DC coupled Doppler radar physiological monitor," in *Annu. IEEE Int. Eng. Med. Biol. Soc. Conf.*, 2011, pp. 1909–1912.

[22] C. Li and J. Lin, "Random body movement cancellation in Doppler radar vital sign detection," *IEEE Trans. Microw. Theory Techn.*, vol. 56, no. 12, pp. 3143–3152, Dec. 2008.

[23] R. Fletcher and H. Jing, "Low-cost differential front-end for Doppler radar vital sign monitoring," in *IEEE MTT-S Int. Microw. Symp. Dig.*, 2009, pp. 1325–1328.

[24] J. H. Oum, D.-W. Kim, and S. Hong, "Two frequency radar sensor for non-contact vital signal monitor," in *IEEE MTT-S Int. Microw. Symp. Dig.*, 2008, pp. 919–922.

[25] A. Wiesner, "A multifrequency interferometric CW radar for vital signs detection," in *IEEE Radar Conf.*, 2009, pp. 1–4.

[26] A. Singh and V. Lubecke, "Respiratory monitoring using a Doppler radar with passive harmonic tags to reduce interference from environmental clutter," in *Annu. IEEE Int. Eng. Med. Biol. Soc. Conf.*, 2009, pp. 3837–3840.

[27] A. Singh and V. Lubecke, "A heterodyne receiver for harmonic Doppler radar cardiopulmonary monitoring with body-worn passive RF tags," in *IEEE MTT-S Int. Microw. Symp. Dig.*, 2010, pp. 1600–1603.

[28] C. Gu, C. Li, J. Lin, J. Long, J. Huangfu, and L. Ran, "Instrument-based noncontact Doppler radar vital sign detection system using heterodyne digital quadrature demodulation architecture," *IEEE Trans. Instrum. Meas.*, vol. 59, no. 6, pp. 1580–1588, Jun. 2010.

[29] A. D. Droitcour, O. Boric-Lubecke, V. M. Lubecke, and L. Jenshan, "0.25 μm CMOS and BiCMOS single-chip direct-conversion Doppler radars for remote sensing of vital signs," in *IEEE Int. Solid-State Circuits Conf. Tech. Dig.*, 2002, vol. 1, pp. 348–349.

[30] A. D. Droitcour, O. Boric-Lubecke, V. M. Lubecke, J. Lin, and G. T. A. Kovacs, "Range correlation and I/Q performance benefits in single-chip silicon Doppler radars for noncontact cardiopulmonary monitoring," *IEEE Trans. Microw. Theory Tech.*, vol. 52, no. 3, pp. 838–848, Mar. 2004.

[31] C. Li, X. Yu, C.-M. Lee, D. Li, L. Ran, and J. Lin, "High-sensitivity software-configurable 5.8-GHz radar sensor receiver chip in 0.13-μm CMOS for noncontact vital sign detection," *IEEE Trans. Microw. Theory Tech.*, vol. 58, no. 5, pp. 1410–1419, May 2010.

[32] C. Li, Y. Xiao, and J. Lin, "A 5 GHz double-sideband radar sensor chip in 0.18 μm CMOS for non-contact vital sign detection," *IEEE Microw. Wireless Compon. Lett.*, vol. 18, no. 7, pp. 494–496, Jul. 2008.

[33] C. Li and J. Lin, "Optimal carrier frequency of non-contact vital sign detectors," in *IEEE Radio Wireless Symp.*, 2007, pp. 281–284.

[34] D. T. Petkie, C. Benton, and E. Bryan, "Millimeter wave radar for remote measurement of vital signs," in *IEEE Radar Conf.*, 2009, pp. 1–3.

[35] C. Huey-Ru, K. Hsin-Chih, L. Fu-Ling, H. Tzuen-Hsi, K. Chi-Shin, and O. Ya-Wen, "60-GHz millimeter-wave life detection system (MLDS) for noncontact human vital-signal monitoring," *IEEE Sens. J.*, vol. 12, no. 3, pp. 602–609, Mar. 2012.

[36] S. Bakhtiari *et al.*, "Compact millimeter-wave sensor for remote monitoring of vital signs," *IEEE Trans. Instrum. Meas.*, vol. 61, no. 3, pp. 830–841, Mar. 2012.

[37] I. V. Mikhelson, P. Lee, S. Bakhtiari, T. W. Elmer, A. K. Katsaggelos, and A. V. Sahakian, "Noncontact millimeter-wave real-time detection and tracking of heart rate on an ambulatory subject," *IEEE Trans. Inform. Technol. Biomed.*, vol. 16, no. 5, pp. 927–934, Jun. 2012.

[38] A. J. Gatesman *et al.*, "Terahertz behavior of optical components and common materials—Art. no. 62120E," *Terahertz Military Security Appl. IV*, vol. 6212, pp. E2120–E2120, 2006.

[39] C. Li and J. Lin, "Complex signal demodulation and random body movement cancellation techniques for non-contact vital sign detection," in *IEEE MTT-S Int. Microw. Symp. Dig.*, 2008, pp. 567–570.

[40] C. Li, Y. Xiao, and J. Lin, "Experiment and spectral analysis of a low-power Ka-band heartbeat detector measuring from four sides of a human body," *IEEE Trans. Microw. Theory Techn.*, vol. 54, no. 12, pp. 4464–4471, Dec. 2006.

[41] M. C. Budge, Jr. and M. P. Burt, "Range correlation effects on phase and amplitude noise," in *Proc. IEEE Southeastcon'93*, 1993, p. 5.

[42] A. Droitcour, V. Lubecke, L. Jenshan, and O. Boric-Lubecke, "A microwave radio for Doppler radar sensing of vital signs," in *IEEE MTT-S Int. Microw. Symp. Dig.*, 2001, vol. 1, pp. 175–178.

[43] Y. Xiao, L. Jenshan, O. Boric-Lubecke, and V. M. Lubecke, "A Ka-band low power Doppler radar system for remote detection of cardiopulmonary motion," in *27th Annu. Int. Eng. Med. Biol. Soc. Conf.*, 2005, pp. 7151–7154.

[44] Y. Xiao, J. Lin, O. Boric-Lubecke, and M. Lubecke, "Frequency-tuning technique for remote detection of heartbeat and respiration using low-power double-sideband transmission in the Ka-band," *IEEE Trans. Microw. Theory Techn.*, vol. 54, no. 5, pp. 2023–2032, May 2006.

[45] R. Moraes and D. H. Evans, "Compensation for phase and amplitude imbalance in quadrature Doppler signals," *Ultrasound Med. Biol.*, vol. 22, pp. 129–137, 1996.

[46] C. Z. Gu, J. Long, J. T. Huangfu, S. Qiao, W. Z. Cui, W. Ma, and L. X. Ran, "An instruments-built Doppler radar for sensing vital signs," in *Proc. 8th Int. Antennas, Propag., EM Theory Symp.*, 2008, vol. 1–3, pp. 1386–1389.

[47] I. Mostafanezhad, O. Boric-Lubecke, and V. Lubecke, "A coherent low IF receiver architecture for Doppler radar motion detector used in life signs monitoring," in *IEEE Radio Wireless Symp.*, 2010, pp. 571–574.

[48] X. Yu, C. Li, and J. Lin, "Two-dimensional noncontact vital sign detection using Doppler radar array approach," in *IEEE MTT-S Int. Microw. Symp. Dig.*, 2011, pp. 1–4.

[49] I. Mostafanezhad, O. Boric-Lubecke, V. Lubecke, and D. P. Mandic, "Application of empirical mode decomposition in removing fidgeting interference in Doppler radar life signs monitoring devices," in *Annu. IEEE Int. Eng. Med. Biol. Soc. Conf.*, 2009, pp. 340–343.

[50] I. Mostafanezhad, O. Boric-Lubecke, V. Lubecke, and A. Host-Madsen, "Cancellation of unwanted motion in a handheld Doppler radar used for non-contact life sign monitoring," in *IEEE MTT-S Int. Microw. Symp. Dig.*, 2008, pp. 1171–1174.

[51] Q. Zhou, J. H. Liu, A. Host-Madsen, O. Boric-Lubecke, and V. Lubecke, "Detection of multiple heartbeats using Doppler radar," in *Proc. IEEE Int. Acoust., Speech, Signal Process. Conf.*, 2006, vol. II, pp. 1160–1163.

[52] A. Vergara, N. Petrochilos, O. Boric-Lubecke, A. Host-Madsen, and V. Lubecke, "Blind source separation of human body motion using direct conversion Doppler radar," in *IEEE MTT-S Int. Microw. Symp. Dig.*, 2008, pp. 1321–1324.

[53] A. Host-Madsen, N. Petrochilos, O. Boric-Lubecke, V. M. Lubecke, B. K. Park, and Q. Zhou, "Signal processing methods for Doppler radar heart rate monitoring," in *Signal Processing Techniques for Knowledge Extraction and Information Fusion*, D. Mandic, Ed.   Berlin, Germany: Springer-Verlag, 2008.

[54] D. Samardzija, B.-K. Park, V. M. Lubecke, O. Boric-Lubecke, V. Lubecke, and T. Sizer, "Experimental evaluation of multiple antenna techniques for remote sensing of physiological motion," in *IEEE MTT-S Int. Microw. Symp. Dig.*, 2007, pp. 1735–1738.

[55] A. D. Droitcour, O. Boric-Lubecke, V. M. Lubecke, J. Lin, and G. T. A. Kovacs, "Range correlation effect on ISM band I/Q CMOS radar for non-contact vital signs sensing," in *IEEE MTT-S Int. Microw. Symp. Dig.*, 2003, vol. 3, pp. 1945–1948.

[56] T. Y. J. Kao, A. Y. K. Chen, Y. Yan, S. Tze-Min, and L. Jenshan, "A flip-chip-packaged and fully integrated 60 GHz CMOS micro-radar sensor for heartbeat and mechanical vibration detections," in *IEEE Radio Freq. Integr. Circuits Symp.*, 2012, pp. 443–446.

[57] A. Singh and V. M. Lubecke, "Respiratory monitoring and clutter rejection using a CW Doppler radar with passive RF tags," *IEEE Sens. J.*, vol. 12, no. 3, pp. 558–565, Mar. 2012.

[58] A. Singh and V. Lubecke, "Adaptive noise cancellation for two frequency radars using frequency doubling passive RF tags," in *IEEE MTT-S Int. Microw. Symp. Dig.*, 2012, pp. 1–3.

[59] I. Mostafanezhad and O. Boric-Lubecke, "An RF based analog linear demodulator," *IEEE Microw. Wireless Compon. Lett.*, vol. 21, no. 7, pp. 392–394, Jul. 2011.

[60] W. Pan, J. Wang, J. Huangfu, C. Li, and L. Ran, "Null point elimination using RF phase shifter in continuous-wave Doppler radar system," *Electron. Lett.*, vol. 47, pp. 1196–1198, 2011.

[61] F. K. Wang *et al.*, "An injection-locked detector for concurrent spectrum and vital sign sensing," in *IEEE MTT-S Int. Microw. Symp. Dig.*, 2010, pp. 768–771.

[62] C. J. Li, F. K. Wang, T. S. Horng, and K. C. Peng, "A novel RF sensing circuit using injection locking and frequency demodulation for cognitive radio applications," *IEEE Trans. Microw. Theory Techn.*, vol. 57, no. 12, pp. 3143–3152, Dec. 2009.

[63] F.-K. Wang *et al.*, "A novel vital-sign sensor based on a self-injection-locked oscillator," *IEEE Trans. Microw. Theory Tech.*, vol. 58, no. 12, pp. 4112–4120, Dec. 2010.

[64] F.-K. Wang, T.-S. Horng, K.-C. Peng, J.-K. Jau, J.-Y. Li, and C.-C. Chen, "Single-antenna Doppler radars using self and mutual injection locking for vital sign detection with random body movement cancellation," *IEEE Trans. Microw. Theory Techn.*, vol. 59, no. 12, pp. 3577–3587, Dec. 2011.

[65] L. Marechal, C. Barthod, L. Goujon, and T. Bussing, "Design and development of a mechatronic infant torso simulator for respiratory physiotherapy learning," *Mechatronics*, vol. 22, pp. 55–64, Feb. 2012.

[66] J. W. Herrman, J. K. Waterhouse, and J. Chiquoine, "Evaluation of an infant simulator intervention for teen pregnancy prevention," *J. Obstet. Gynecol. Neonat. Nursing*, vol. 40, pp. 322–328, May–Jun. 2011.

[67] J. T. Zoldak *et al.*, "An electronic simulator for testing infant apnoea monitors that uses actual physiologic data," *Physiol. Meas.*, vol. 22, pp. N1–N12, May 2001.

[68] Y. Yan, C. Li, X. Yu, M. D. Weiss, and J. Lin, "Verification of a non-contact vital sign monitoring system using an infant simulator," in *Annu. IEEE Int. Eng. Med. Biol. Soc. Conf.*, 2009, pp. 4836–4839.

[69] A. Nezirovic, A. G. Yarovoy, and L. P. Ligthart, "Experimental study on human being detection using UWB radar," in *Int. Radar Symp.*, 2006, pp. 1–4.

[70] Y. Yunqiang and A. E. Fathy, "Development and implementation of a real-time see-through-wall radar system based on FPGA," *IEEE Trans. Geosci. Remote Sens.*, vol. 47, no. 5, pp. 1270–1280, May 2009.

[71] Z. Zhu, X. Zhang, H. Lv, G. Lu, X. Jing, and J. Wang, "Human-target detection and surrounding structure estimation under a simulated rubble via UWB radar," *IEEE Geosci. Remote Sens. Lett.*, vol. 10, no. 2, pp. 328–331, Mar. 2013.

[72] W. Li, H. Lv, G. Lu, Y. Zhang, X. Jing, S. Li, and J. Wang, "A new method for non-line-of-sight vital sign monitoring based on developed adaptive line enhancer using low centre frequency UWB radar," *Progr. Electromagn. Res.*, vol. 133, pp. 535–554, 2013.

[73] A. G. Stove, "Linear FMCW radar techniques," *Proc. Inst. Elect. Eng. –Radar Signal Process.*, vol. 139, pt. F, pp. 343–350, 1992.

[74] R. Feger, A. Haderer, S. Schuster, S. Scheiblhofer, and A. Stelzer, "A four channel 24-GHz FMCW radar sensor with two-dimensional target localization capabilities," in *IEEE MTT-S Int. Microw. Symp. Dig.*, 2008, pp. 125–128.

[75] N. Maaref, P. Millot, C. Pichot, and O. Picon, "A study of UWB FM-CW Radar for the detection of human beings in motion inside a building," *IEEE Trans. Geosci. Remote Sens.*, vol. 47, no. 5, pp. 1297–1300, May 2009.

[76] Y. Wang, Q. Liu, and A. E. Fathy, "CW and pulse–Doppler radar processing based on FPGA for human sensing applications," *IEEE Trans. Geosci. Remote Sens.*, to be published.

Changzhi Li (S'06–M'09) received the B.S. degree in electrical engineering from Zhejiang University, Hangzhou, China, in 2004, and the M.S. and Ph.D. degrees in electrical engineering from the University of Florida, Gainesville, FL, USA, in 2007 and 2009, respectively

In the summers of 2007–2009, he was with Alereon Inc., Austin, TX, USA, and Coherent Logix Inc., Austin, TX, USA, where he was involved with UWB and software-defined radar. In August 2009, he joined Texas Tech University, Lubbock, TX, USA, as an Assistant Professor. His research interests include biomedical applications of microwaves/RF, wireless sensors, frequency synthesizers, and microwave/millimeter-wave circuits.

Dr. Li was the Technical Program Committee (TPC) co-chair for IEEE WAMICON 2012 and 2013. He was the recipient of the National Science Foundation (NSF) Faculty Early CAREER Award in 2013, the Texas Tech Alumni Association New Faculty Award in 2012, and the IEEE Microwave

Theory and Techniques Society (IEEE MTT-S) Graduate Fellowship Award in 2008. He was also the recipient of seven Best Conference/Student Paper Awards as an author/advisor of IEEE Radio and Wireless Week (RWW) and the IEEE Wireless and Microwave Technology Conference (WAMICON). He was the finalist of the Vodafone Wireless Innovation Project competition in 2011.

Victor M. Lubecke (S'86–M'86–SM'98) received the B.S.E.E. degree from the California State Polytechnic Institute, Pomona, CA, USA, in 1986, and the M.S. and Ph.D. degrees in electrical engineering from the California Institute of Technology, Pasadena, CA, USA, in 1990 and 1995, respectively.

He is currently a Professor of electrical engineering with the University of Hawaii at Manoa, Honolulu, HI, USA. He has held previous appointments with Bell Laboratories, Lucent Technologies (1998–2003), the National Aeronautics and Space Administration (NASA) Jet Propulsion Laboratory (JPL) (1987–1996), and the Institute for Physical and Chemical Research (RIKEN), Sendai, Japan (1996–1998). He cofounded and served as Chief Technical Officer (CTO) for the startup company Kai Medical, Honolulu, HI, USA. He has authored or coauthored over 150 peer-reviewed research papers. He holds six U.S. patents with several more pending. His research has involved microwave, terahertz, and microelectromechanical systems (MEMS) technologies for remote sensing and communications. His current research interests include remote sensing technologies, biomedical sensors, MEMS, heterogeneous integration, and microwave/terahertz radio.

Prof. Lubecke is an emeritus Distinguished Microwave Lecturer (2006–2008) of the IEEE Microwave Theory and Techniques Society (IEEE MTT-S). He is a member of the IEEE Engineering in Medicine and Biology Society and Electron Devices Society. He serves on the Technical Committee and Steering Committee for various IEEE and SPIE symposia. He was a corecipient of the Emerging Technology Award at TechConnect 2007.

Olga Boric-Lubecke (S'90–M'90–SM'01) received the B.Sc. degree from the University of Belgrade, Belgrade, Yugoslavia, in 1989, the M.S. degree from the California Institute of Technology, Pasadena, CA, USA, in 1990, and the Ph.D. degree from the University of California at Los Angeles (UCLA), Los Angeles, CA, USA, in 1995, all in electrical engineering.

She is currently a Professor of electrical engineering with the University of Hawaii at Manoa, Honolulu, HI, USA. From 1998 to 2003, she was with Bell Laboratories, Lucent Technologies, Murray Hill, NJ, USA, where she conducted research in RF integrated circuit technology and biomedical applications of wireless systems. Prior to that, she held appointments with the Institute for Physical and Chemical Research, Sendai, Japan (1996–1998), and the National Aeronautics and Space Administration (NASA) Jet Propulsion Laboratory, Pasadena, CA, USA (1995–1996). She cofounded and is the Chief Technical Advisor for Kai Medical Inc. She has authored or coauthored over 150 journal and conference publications. Her current research interests include silicon RF integrated circuits, high-frequency integrated circuits, biomedical applications, and renewable energy. Her current research interests include silicon RF integrated circuits, high-frequency integrated circuits, biomedical applications, and renewable energy. Her research has been featured in various newspapers, magazines, and radio programs.

Dr. Boric-Lubecke serves on the Technical Program Committee and Steering Committee for various IEEE and SPIE symposia. She was the workshop chair for the 2003 IEEE Microwave Theory and Techniques Society (IEEE MTT-S) International Microwave Symposium (IMS). She was Technical Program vice-chair for the 2007 IEEE MTT-S IMS. She is currently an associate editor for IEEE MICROWAVE AND WIRELESS COMPONENTS LETTERS and an associate editor for the IEEE Engineering in Medicine and Biolology Soceity Conference (EMBC). She was the corecipient of the Emerging Technology Award at TechConnect 2007. She was the advisor–author of several award winning IEEE MTT-S and EMBS student papers.

Jenshan Lin (S'91–M'94–SM'00–F'10) received the Ph.D. degree in electrical engineering from the University of California at Los Angeles (UCLA), Los Angeles, CA, USA, in 1994.

He was with AT&T Bell Labs (which later became Lucent Bell Labs), Murray Hill, NJ, USA, from 1994 to 2001, and its spin-off Agere Systems from 2001 to 2003. In July 2003, he joined the University of Florida, Gainesville, FL, USA, as an Associate Professor and became a Professor in August 2007. He was a Visiting Professor with National Taiwan University in the summer of 2006, a Visiting Researcher with NTT, Atsugi, Japan, during the summer of 2010, and a Visiting Chair Professor with National Sun Yat-Sen University, Taiwan, in the summer of 2012. He has authored or coauthored over 220 technical publications in refereed journals and conferences proceedings, and holds ten U.S. patents. His research interests include sensors and biomedical applications of microwave and millimeter-wave technologies, and wireless power transmission.

Dr. Lin has served on several committees in the IEEE Microwave Theory and Techniques Society (IEEE MTT-S). From 2006 to 2011, he was an elected member of the IEEE MTT-S Administrative Committee (AdCom), where he served as the chair of Technical Coordinating Committee from 2010 to 2011. He served as an associate editor for the IEEE TRANSACTIONS ON MICROWAVE THEORY AND TECHNIQUES from 2006 to 2010. He has been a member of several conference committees, including the IEEE MTT-S International Microwave Symposium (IMS), the Radio Frequency Integrated Circuits Symposium (RFIC), the Radio and Wireless Symposium (RWS), and the Asia–Pacific Microwave Conference (APMC). He was the general chair of the 2008 RFIC Symposium, the Technical Program chair of the 2009 Radio and Wireless Symposium, and the General co-chair of the 2012 Asia–Pacific Microwave Conference. He was the recipient of the 1994 UCLA Outstanding Ph.D. Award, the 1997 Eta Kappa Nu Outstanding Young Electrical Engineer Honorable Mention Award, and the 2007 IEEE MTT-S N. Walter Cox Award.